Structure and mechanism of the UvrA–UvrB DNA damage sensor

Danaya Pakotiprapha, Martin Samuels, Koning Shen, Johnny H Hu & David Jeruzalmi

Nucleotide excision repair (NER) is used by all organisms to eliminate DNA lesions. We determined the structure of the *Geobacillus stearothermophilus* UvrA–UvrB complex, the damage-sensor in bacterial NER and a new structure of UvrA. We observe that the DNA binding surface of UvrA, previously found in an open shape that binds damaged DNA, also exists in a closed groove shape compatible with native DNA only. The sensor contains two UvrB molecules that flank the UvrA dimer along the predicted path for DNA, ~80 Å from the lesion. We show that the conserved signature domain II of UvrA mediates a nexus of contacts among UvrA, UvrB and DNA. Further, in our new structure of UvrA, this domain adopts an altered conformation while an adjacent nucleotide binding site is vacant. Our findings raise unanticipated questions about NER and also suggest a revised picture of its early stages.

It is estimated that human cells experience thousands of DNA-damaging events per day. Exposure to UV radiation from sunlight accounts for a substantial percentage of these events and makes the resulting cancers of the skin the most common cancers worldwide[1]. Absorption of UV radiation leads to accumulation of covalent links between adjacent pyrimidines (cyclobutane pyrimidine dimers and (6-4) adducts, **Fig. 1a**) on one strand of DNA. DNA damaged in this way must be repaired to prevent disease, and the NER pathway is the only known mechanism in human cells that removes these lesions[2]. More than a dozen proteins operate in this pathway to identify lesions, excise damaged segments and restore the original DNA sequence[3]. Mutations in the human NER pathway can cause xeroderma pigmentosum, a disease associated with a 2,000-fold higher incidence of skin cancer[4].

In bacteria, the NER pathway is implemented by the successive action of three proteins, UvrA, UvrB and UvrC, through a series of large and dynamic multiprotein complexes[5]. A large number of genetic and biochemical studies have defined three major stages associated with the early steps of the NER pathway (**Fig. 1b**). In stage 1, a large (300–400 kDa) UvrA–UvrB complex (also referred to below as the AB complex) scans the genome to identify lesion-containing DNA. This process requires rapid binding and release of DNA; moreover, damage must be specifically recognized and distinguished from native DNA, despite the fact that the relevant lesions induce widely different DNA structures (**Fig. 1a**). Once lesion-containing DNA has been located, it is stably bound by a dimeric form of UvrA within the AB complex (stage 2). A major reorganization then occurs in which UvrA is lost from the ensemble, and concomitantly, UvrB becomes localized at the site of damage (stage 3)[6]. Following these early stages, additional events lead to excision of the damage on one strand and repair of the resulting single-stranded gap (reviewed in ref. 5). Biochemical studies of bacterial NER have provided important

paradigms for understanding the eukaryotic pathway, which, although more elaborate, broadly implements the same sequence of events.

Previous structural studies have provided insights into how lesion DNA is stably bound by UvrA at stage 2 (ref. 7) and into the binding of UvrB to single-stranded DNA during stage 3 (refs. 8–10). Although highly informative, these studies leave important questions unanswered. Among these are (i) how does genome scanning occur; most importantly, how are diverse damaged DNA substrates (**Fig. 1a**) specifically recognized, while being distinguished from the vast excess of native DNA (**Fig. 1b**, stage 1); and (ii) during the transition to stage 3, concomitant with loss of UvrA from the complex, UvrB becomes localized to the site of damage; where is UvrB before this transition, and how is its localization managed in time and space?

Here we focus on the molecular mechanisms of protein complexes that operate during the three early stages of NER and on the transitions that link one stage to the next (**Fig. 1b**). We report the first structure of the UvrA–UvrB complex, along with complementary mutational, biochemical and modeling studies. In addition, we describe a new structure of the UvrA dimer that is unique in both nucleotide composition and in the conformation of a highly conserved domain implicated in nucleotide-mediated structural changes in ABC ATPases (signature domain II). The results provide insights into all three major early stages of NER, thus permitting a coherent view of this portion of the reaction pathway.

RESULTS

Overall nature of the UvrA–UvrB complex

We have determined the first structure of the UvrA–UvrB complex (**Table 1**). The complex crystallized with one AB heterodimer in the asymmetric unit. As UvrA is known to be a dimer[6,11], the complete sensor was generated by application of a crystallographic two-fold axis. This yields a $UvrA_2–UvrB_2$ entity with two UvrB molecules located

Figure 1 Deformed DNA conformations processed by NER. (**a**) Examples of DNA lesions processed by bacterial NER: cyclobutane pyrimidine dimer, benzo[*a*]pyrene and acetylaminofluorene (PDB 1N4E[43], 1DXA[44] and 2GE2 (ref. 45), respectively). Lesions are shown in orange and the deformed DNA duplexes in cyan. As a reference, an ideal B-form DNA (gray), with its helical axis highlighted, is shown superimposed. (**b**) The overall mechanism of bacterial NER. UvrA, within the AB sensor, searches for deformed, damaged DNA. The lesion is represented by a red star.

on either side of the central UvrA dimer (**Fig. 2**). We confirm this arrangement and stoichiometry in solution (see below).

The overall shape of the AB complex is reminiscent of a Venetian gondola, with overall dimensions of $80 \times 90 \times 210$ Å and a deep and narrow groove that traverses ~145 Å (measured between the Cα atoms of Tyr95 of the two UvrB molecules) through the entire length of the complex (**Fig. 2** and discussed below). The dimensions of this groove suggest that it could readily bind ~45 base pairs (bp) of B-form DNA, ~32 bp of which are contained within the UvrA dimer. These lengths compare well with values obtained from DNase I footprints of the AB complex (~45 bp) and UvrA (~33 bp), respectively[12]. Also, the portion of this groove that lies within the two UvrB protomers corresponds directly to the known path of DNA through UvrB[8] (**Fig. 3**). However, the trajectory of DNA through the complex will probably deviate from B-form DNA. These considerations imply that the elongated UvrB–UvrA–UvrA–UvrB heterotetramer could be associated with DNA along its entire length.

UvrA specifies two distinct types of ABC-style ATP binding sites, designated 'proximal' and 'distal'. The UvrA dimer thus harbors two copies of each type of site[7,13–15]. A complete description of the ATPase sites and domain architecture of UvrA appears in the **Supplementary Discussion** and **Supplementary Figure 1** and, more completely, in ref. 13. UvrB contains one ATP binding site, which is associated with its helicase and single-stranded DNA translocase activity[16]. Thus, the A_2B_2 complex in our structure contains a total of six nucleotide binding sites, each of which is occupied (**Supplementary Fig. 2**). The resolution of our diffraction data (4.4 Å), however, does not permit unambiguous identification of the nucleotide in each site.

UvrA adopts a 'closed' DNA binding surface in the AB complex

In the AB complex presented here, the conformation of the central UvrA dimer differs substantially from that previously described[7,13–15], with important implications for the DNA binding surface. Superposition of the two distinct types of dimers reveals that a 25° helical rigid body rotation (~25° rotation and ~10-Å translation) of each UvrA protomer is required to bring UvrA from the AB complex into alignment with the previously described dimer (**Fig. 3c,d** and **Supplementary Movies 1** and **2**). A consequence of this transformation is that the two distinct types of dimers are held together by quite different interfaces. Furthermore, the observed structural change is only apparent in the context of the UvrA dimer; the structures of the individual protomers closely resemble each other. Superposition of all available protomers (PDB 2R6F, 2VF7, 2VF8, 3PIH and 3ZQJ)[7,13–15] onto UvrA from the AB complex shows an average r.m.s. deviation of 1.2 Å measured between Cα atoms contained within the two nucleotide binding domains. Moreover, because the axis of the helical rotation between the two types of dimers corresponds roughly to the path of DNA through the AB complex, as inferred from the structure of the UvrA–DNA complex[7], an important overall consequence is that the two configurations differ substantially in the nature of their DNA binding surfaces (**Fig. 3**). The conformation seen in the previously described UvrA dimer is an open, relatively flat, 'tray-like' surface (~43 Å wide, ~25 Å deep and ~100 Å long)[7,13–15]. Thus, this conformation is designated the 'open
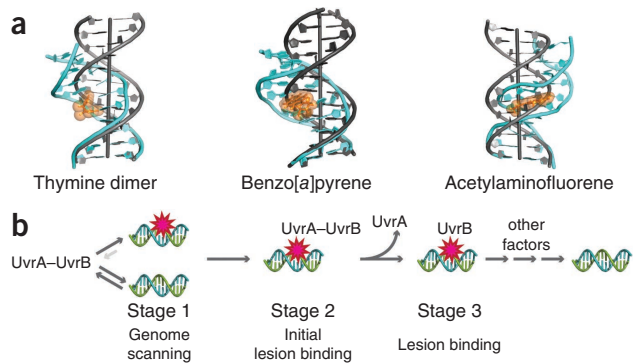
tray' conformation. By contrast, the corresponding DNA binding surface in the UvrA dimer from the AB complex comprises a deep and narrow channel, ~30 Å in both depth and width, and represents a closed state. Accordingly, we designate this state as the 'closed groove' form.

The difference in shape between the closed groove and open tray dimer configurations has implications for the interactions that UvrA makes with DNA. Modeling studies show that although the closed groove conformation of UvrA can accommodate native B-form DNA, it cannot accommodate DNA that is damaged by three lesions processed by the NER pathway: thymine dimer, benzo[*a*]pyrene or acetylaminofluorene (**Fig. 1a**). None of these lesion DNAs can be positioned in the deep, narrow groove of UvrA in the AB complex without severe clashes (**Fig. 4** and data not shown). By contrast, the open tray conformation of UvrA is known to bind damaged DNA, with the lesion itself localized to a site approximately in the center of the UvrA dimer[7]. Moreover, a parallel modeling analysis shows that the DNA binding surface of the open tray configuration can accommodate not only the

Table 1 Data collection and refinement statistics

	UvrA–UvrB complex	UvrA Δ118–419
Data collection		
Space group	$P4_22_12$	$C2$
Cell dimensions		
a, *b*, *c* (Å)	216.8, 216.8, 116.8	128.7, 51.3, 112.4
α, β, γ (°)	90.0, 90.0, 90.0	90.0, 97.3, 90.0
Resolution (Å)	50.0–4.40 (4.56–4.40)	50.0–2.10 (2.18–2.10)
R_{sym}	10.1 (96.2)	5.6 (40.0)
$I / \sigma I$	21.6 (1.8)	16.1 (2.2)
Completeness (%)	96.6 (82.7)	98.6 (98.8)
Redundancy	8.7 (6.7)	3.3 (3.3)
Refinement		
Resolution (Å)	38.6–4.40	37.1–2.10
No. reflections	17,600	38,318
R_{work} / R_{free}	28.76 / 34.86	21.05 / 24.53
No. atoms		
Protein	12,190	4,339
Ligand/ion	3	28
Water	0	201
B-factors		
Protein	347.3	37.88
Ligand/ion	550.0	45.58
Water		40.92
R.m.s. deviations		
Bond lengths (Å)	0.005	0.008
Bond angles (°)	0.793	1.257

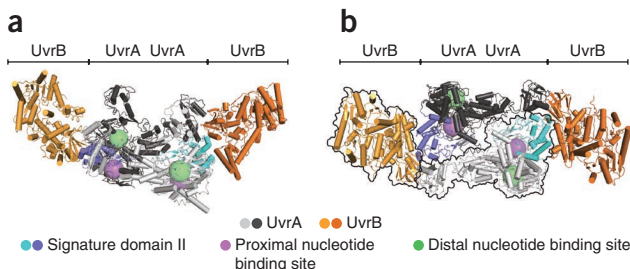Data were collected from one crystal for each structure. Values in parentheses are for highest-resolution shell.

Figure 2 Architecture of the UvrA–UvrB DNA damage sensor. (**a**,**b**) The AB damage sensor is shown as a cartoon in two different views. The view in **a** is related to that in **b** by a 90° rotation about the horizontal *x* axis. The two protomers of UvrA are shown in different shades of gray, with the signature domain II in cyan and blue. UvrB molecules are shown in different shades of orange. The positions of proximal and distal nucleotide binding sites are denoted by semi-transparent magenta and green spheres, respectively. In panel **b**, the boundaries of UvrA and UvrB are outlined.

relatively straight fluorescein lesion substrate described in the structural analysis but also the three other lesions listed above, which confer much more marked distortions (**Fig. 4** and data not shown).

We further defined the DNA binding surface of UvrA by mutating residues. To this end, we chose residues for mutation by inspecting the surface for regions of positive electrostatic potential and sequence conservation. In addition, we mutated residues previously implicated in DNA binding, namely those in the highly conserved signature domain II (ref. 13), in the insertion domain[14,17] and in the three zinc-containing structural modules[5,13,18]. Finally, we also targeted basic residues on the signature domain I (a complete list of positions mutated in this study appears in **Supplementary Table 1**). We compared the mutant and wild-type proteins for their binding affinities for fluorescein-containing DNA by an electrophoretic mobility shift assay (**Fig. 3a**). The results revealed two spatially distinct regions of UvrA that make contacts to lesion DNA (**Fig. 3b**). One group of residues is found in a region along the signature domain II and includes Arg708, which is critical for DNA binding (Region I, blue in **Fig. 3b**). A second group, which is generally less critical for binding, forms a surface patch created by the juxtaposition of residues from several other domains (insertion, zinc-binding and signature domain I) (Region II, pink in **Fig. 3b**).

The closed groove and open tray dimer configurations of UvrA show markedly different dispositions of these two DNA binding regions, further documenting important differences in their DNA binding modes (**Fig. 3c,d**). In the closed groove form, residues from Region I are found at the bottom of the deep groove that runs through the entire length of the complex, whereas Region II residues are observed to line the sides of the groove. By contrast, in the open tray state, both regions lie on the edges of the wide, shallow, square, tray-like DNA binding surface.

The results described above reveal that the UvrA dimer can exist in two distinct configurations that present quite different DNA binding surfaces. The two UvrA dimer states can be interconverted by a simple helical rotation of each protomer along a shared axis that runs along the DNA binding surface. Furthermore, the closed groove dimer defined by the AB structure is capable of binding native DNA but not lesion DNA. By contrast, the open tray configuration of UvrA can and does bind lesion DNA[7]. To accommodate both sets of findings, we propose that interconversion between the two dimeric forms of UvrA is an important feature of the genome scanning process (see also Discussion below).
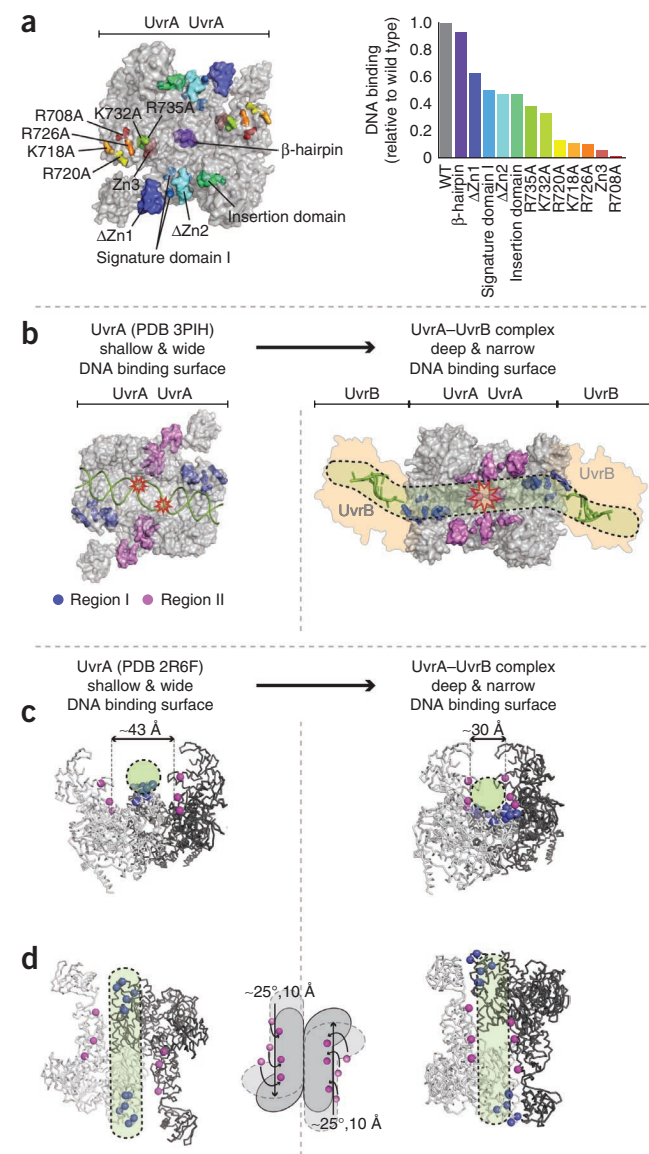

Figure 3 The DNA binding surface of UvrA is composed of two spatially distinct regions and undergoes considerable reconfiguration in the AB sensor. (**a**) Left, residues whose mutation disrupts DNA binding are shown on the surface of the UvrA dimer (PDB 2R6F). For clarity, the location of the mutated residues is indicated on one UvrA protomer. Right, K_a of each mutant for DNA, normalized to that of the wild type. A complete list of UvrA mutants used in this study is in **Supplementary Table 1**. (**b**) The positions analyzed in **a** can be grouped into two spatially distinct regions (Region I in blue and Region II in pink) and are plotted on the surface of the UvrA–DNA complex (PDB 3PIH, left) and the AB sensor (right). The dashed lines on the AB sensor depict the inferred path of DNA through the complex. The red star marks the location of the lesion. (**c**,**d**) Comparison of the two UvrA dimer configurations (left, PDB 2R6F; right, AB complex) in two views. The distances shown in **c** represent the maximal dimension of the DNA binding site in each dimer. Protomers of UvrA (shown in different shades of gray) in the two conformations of the dimer are related by a 25° helical rotation (**d**, 25° rotation, 10-Å translation). Reconfiguration of the UvrA dimer in the AB sensor repositions the Region II DNA binding sites (magenta spheres, Gly258, Asp278 and Arg384) so that they line the side of the DNA binding groove. The predicted path of DNA is shown by dashed lines. The view in **d** is related to that in **c** by a 90° rotation about the *x* axis.

Figure 4 Modeling of native and damaged DNA into the two dimer configurations of UvrA. (**a**) Native DNA was modeled into the DNA binding site of UvrA in the UvrA–DNA complex (PDB 3PIH, left) and into the inferred DNA binding groove of the AB complex (right). (**b**) UvrA bound to fluorescein-containing DNA (PDB 3PIH, left) and thymine dimer–containing DNA modeled into the DNA binding groove of the AB complex (right). In order to make this model, the structure of the thymine (TT) dimer–containing DNA (PDB 1TTD)[46] was extended to 33 bp, which matches the binding site estimated from DNase I footprinting. UvrA and UvrB (gray) and the DNA (cyan) are shown as surfaces. The DNA binding groove is highlighted in green. The TT dimer is shown in orange and the approximate positions of the fluorescein moieties are denoted by stars. Some of the positions implicated as DNA binding residues (Region II) by our study are illustrated using pink filled circles.

a
UvrA (PDB 3PIH)
shallow & wide
DNA binding surface

UvrA–UvrB complex
deep & narrow
DNA binding surface

Native DNA (modeled)

Native DNA (modeled)

b
Fluorescein-containing DNA (PDB 3PIH)

TT dimer–containing DNA (modeled)

Clashes

● DNA binding surface   ● Region II DNA binding sites   ● DNA

Two UvrB molecules bind at the periphery of the UvrA dimer

In the AB complex structure, two UvrB molecules are found at the periphery of the ensemble, flanking the central UvrA dimer, in a linear, two-fold symmetrical UvrB–UvrA–UvrA–UvrB arrangement. Neither the number of UvrB molecules nor their peripheral disposition in the AB complex was anticipated[5]. Although there is wide agreement that UvrA within the complex is dimeric, estimates for the number of UvrB molecules vary. Some studies argue for an A_2B_1 state, whereas others suggest an A_2B_2 state[6,19–22]. To resolve this issue, we carried out two types of studies, which now demonstrate that in solution, the AB complex shows an A_2B_2 stoichiometry and an elongated conformation, consistent with the presented crystal structure.

First, we used small-angle X-ray scattering (SAXS) to construct a low-resolution (22 Å) envelope for the AB complex in solution (unpublished data). This envelope shows an elongated shape of $100 \times 120 \times 180$ Å (**Fig. 5a**). The Guinier approximation[23] and the pair distribution function[24] calculated from the scattering data suggest a radius of gyration (R_g) of 63.8 Å (**Supplementary Fig. 3**). The R_g calculated from our crystal structure closely matches this value (63.6 Å). Furthermore, computational fitting of the crystal structure into the SAXS envelope reveals a satisfactory fit, with a correlation coefficient of ~0.7 (ref. 25 and **Fig. 5a**). Thus, the AB complex shows an elongated conformation in solution, with a composition and shape that matches the one seen in the crystal structure.
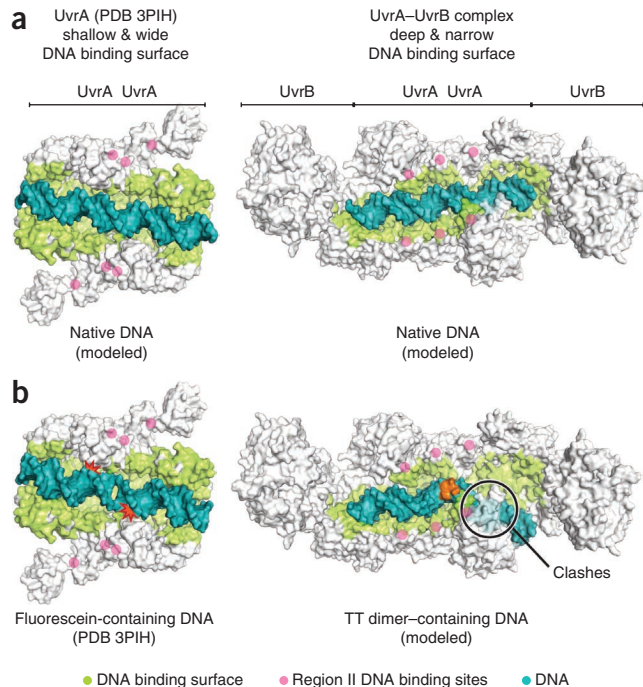
Second, the stoichiometry of the AB complex was evaluated directly by isothermal titration calorimetry in solution. The heat of association during complex formation was measured as UvrB was titrated into a solution of UvrA in the presence of ATP. Analysis of this data, with the 'single set of identical sites' model (Origin 7), revealed a UvrA: UvrB stoichiometry of 1:1 and a dissociation constant of approximately 800 nM (**Fig. 5b** and **Supplementary Fig. 4a**). Given the extensive evidence that UvrA exists as a dimer in solution[6,11], this analysis provides a second line of evidence that the predominant solution state of the AB complex is an A_2B_2 heterotetramer.

Taken together, these results firmly establish that the AB complex in solution exists primarily as an elongated A_2B_2 heterotetramer. These results verify that this state is the relevant form for genome scanning, and they are consistent with conformational switching between the closed groove and open tray forms of UvrA.
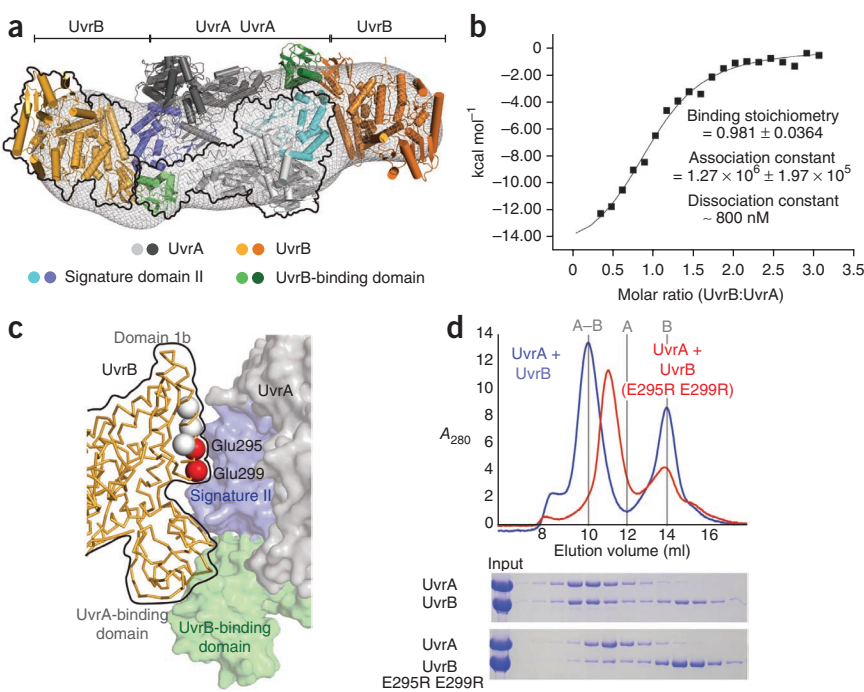

a
UvrB   UvrA UvrA   UvrB

● UvrA   ● UvrB
● Signature domain II   ● UvrB-binding domain

b
Binding stoichiometry = 0.981 ± 0.0364
Association constant = 1.27 × 10⁶ ± 1.97 × 10⁵
Dissociation constant ~ 800 nM

Molar ratio (UvrB:UvrA)

c
Domain 1b
UvrB
UvrA
Glu295
Glu299
Signature II
UvrB-binding domain
UvrA-binding domain

d
A–B   A   B
UvrA + UvrB
UvrA + UvrB (E295R E299R)
A_{280}
Elution volume (ml)
Input
UvrA
UvrB
UvrA
UvrB E295R E299R

Figure 5 Determination of the disposition and number of UvrB molecules in the AB damage sensor. (**a**) The molecular envelope of the AB sensor complex calculated from solution SAXS data is depicted as a gray mesh. For clarity, one copy each of UvrA and UvrB is outlined. (**b**) Isothermal titration calorimetry analysis reveals that the A:B stoichiometry of the complex is 2:2. (**c,d**) The UvrA-UvrB interface seen in the crystal structure (**c**) and its verification by mutation (**d**). UvrB interacts with two distinct regions of the UvrA dimer. Contacts are made between domain 1b of UvrB and the UvrA signature domain II (blue) and between discrete interaction domains in UvrB and UvrA[19]. UvrA is shown as a molecular surface and UvrB is shown as an orange Cα trace. Mutation of two UvrB residues (E295R E299R, red spheres in panel **c**) weakened interaction between UvrA and UvrB, as assessed by size-exclusion chromatography (**d**). A complete list of UvrB residues mutated in this study appears in **Supplementary Table 1**.

Figure 6 Structure of UvrA in a unique domain conformation and its implications for dynamic contacts in the AB–DNA complex. (**a**) The structure of UvrA Δ118–419 shows an asymmetric occupancy of nucleotide binding sites (transparent yellow circles, D = ADP, X = unoccupied). Dotted lines show regions of the structure (tips of the UvrA β-hairpin) that are not included in the model owing to poor order in the crystal. (**b**) Closeup view of the two types of nucleotide binding sites (proximal and distal) in UvrA Δ118–419. The difference electron density, calculated without ADP and contoured at 3σ, is shown as a blue mesh. The structural elements characteristic of ABC ATPases (Walker A, Walker B and ABC signature motifs) are in color. (**c**) Pairwise structural comparisons of the three conformations of UvrA protomers. R.m.s. deviations of each pair are plotted as a function of the amino acid index. Changes between the structure of UvrA and UvrA Δ118–419 are localized to signature domain II and are highlighted in cyan. Changes between isolated UvrA and UvrA within the AB complex are localized to the UvrB-binding domain (highlighted in gray). (**d**) Mutation of the proximal site (K37A) partially disrupts UvrA-UvrB interaction as assessed by size-exclusion chromatography. Elution positions of the wild-type AB complex and the isolated proteins are indicated by gray lines. SDS-PAGE analysis of the column fractions confirms the identity of the indicated peaks. (**e**) Structural comparison of UvrA (PDB 2R6F) and UvrA Δ118–419. The signature domain II undergoes a rigid body rotation of ~16° upon going from the conformation in the UvrA structure (cyan) to that in the UvrA Δ118–419 structure (magenta). This structural change alters the distance between the DNA binding residues in the two protomers (for example, Lys718, black spheres) such that in the UvrA Δ118–419 conformation, the protein is likely to be incompetent to bind DNA. The regions of the structure that do not substantially change are shown in gray, and part of the structure is omitted for clarity. Cartoon representations of the conformational changes are shown below the molecular images. (**f**) Structural comparison of UvrA in the AB complex and UvrA Δ118–419. The structures were superimposed on the ATP binding domain I. Cartoon representations of the conformational changes are shown below the molecular images.
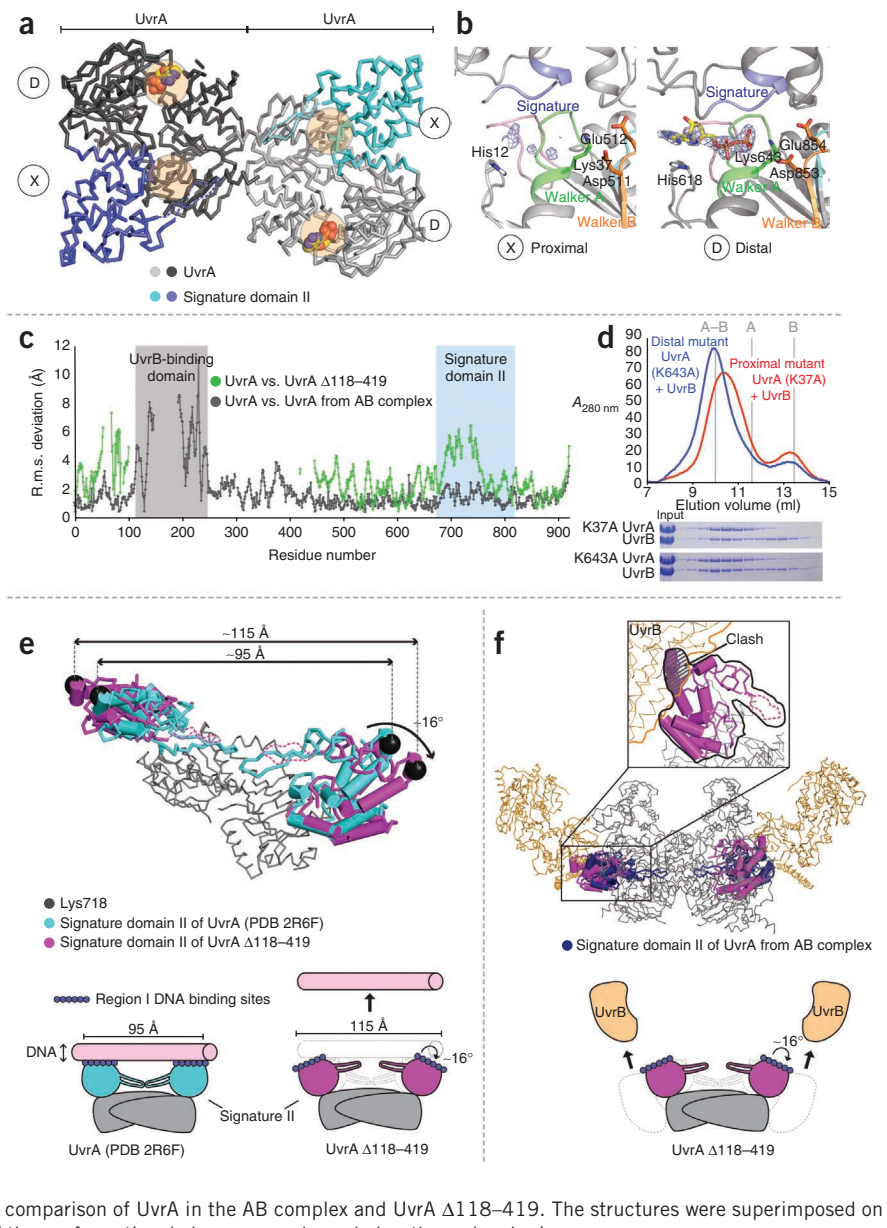
Furthermore, we conclude that, after binding to a DNA lesion, UvrB within the AB complex is not located close to the expected position of the lesion[7,12], as was anticipated, but is at a considerable distance (~80 Å). The implications of these findings are discussed below.

UvrA signature domain II: a nexus between UvrB, ATP and DNA
One of the hallmarks of the ABC family of ATPases is their capacity to undergo biochemical cycles of conformational changes coupled to binding, hydrolysis and release of the nucleotide; these conformational changes are directly provoked by changes in the position of the conserved signature domain. Each cycle is accompanied by changes in the spatial arrangement of structural elements that make up the nucleotide binding site. When the nucleotide is bound, one of these elements, the signature domain, associates tightly with its partner, the ATP binding domain. After nucleotide hydrolysis and ADP release, the signature domain loses this tight association and adopts a new conformation that mediates changes to other parts of the protein[26–29]. UvrA possesses two

such domains (I and II) that could undergo conformational switching. Here we focus on the signature domain II, which partners with the ATP binding domain I to give rise to the proximal nucleotide binding site (**Supplementary Fig. 1**). The mutational analysis described above reveals that the signature domain II makes functionally critical contacts to damaged DNA when UvrA is in the open tray state (**Fig. 3** and ref. 7), and our modeling study predicts that there are contacts between this domain and DNA in the closed groove state of UvrA (**Fig. 3**). Inspection of the AB structure further reveals that signature domain II also mediates contacts with UvrB. The interface between UvrB and UvrA is characterized by contacts in two distinct regions (**Fig. 5c**). One of these regions, previously unrecognized, is the interface between the main portion of UvrB and the signature domain II of UvrA. The second region was shown by prior structural and mutational studies as providing important contacts between UvrA and UvrB[19,30].

To test the functional importance of contacts between UvrB and the signature domain II of UvrA, we conducted a mutational study that

targeted residues on the UvrB side of the interface. As our electron density maps did not resolve the protein side chains involved in the interface, we selected five residues, based on the distances between alpha carbon positions (10 Å). Because of the known salt sensitivity of the interaction between UvrA and UvrB[31], we focused our efforts on charged residues. To maximize our chances of disrupting the interface, the selected positions were mutated in groups to residues of opposite charge. As negative controls, we mutated five other charged residues on UvrB, located distant from the interface (**Supplementary Table 1**). Mutant UvrB proteins were tested for interaction with wild-type UvrA by size-exclusion chromatography. We found that one of the UvrB mutations at the new interface, E295R E299R, weakens the interaction with UvrA (**Fig. 5d**). This mutation perturbs, but does not completely disrupt, the UvrA–UvrB complex. This is the expected phenotype because the important contacts between UvrA and UvrB, which reside in the region that we previously described[19,30], remain unaltered. None of the other analyzed mutations had any detectable effect. Thus, the signature domain II is required for stable association of UvrA and UvrB. Furthermore, this analysis provides additional support for the peripheral location of UvrB in the AB complex.

Taken together, the above results reveal that the signature domain II is in a position to mediate nucleotide-dependent conformational changes that alter the relationships among the three molecules in the damage-sensing ensemble that consists of UvrA, UvrB and DNA.

A structure of UvrA with an altered signature domain II

To further probe for nucleotide-dependent conformational changes within UvrA, we specifically sought to determine structures with different occupancies of the nucleotide binding sites than those previously described. Crystallization trials were carried out with several different constructs of UvrA in the presence of ATP and various analogs. The best results were obtained with a version of UvrA missing two flexible domains that could interfere with the formation of highly ordered crystals: UvrA Δ118–419. This UvrA mutant retains both nucleotide binding domains, is a dimer in solution and has DNA binding and ATPase activities (~20% of wild type).

UvrA Δ118–419 crystallized with one copy in the asymmetric unit, and the active dimeric entity was derived by applying a crystallographic two-fold axis. Notably, the relationship between the protomers in this dimer is identical to that seen in the lesion-binding open tray conformation[13]. This new structure closely resembles the previous one in core regions (r.m.s. deviation = 0.6 Å, **Supplementary Discussion**), but it differs substantially from the open tray conformation with respect to two features.

First, the signature domain II–associated proximal nucleotide binding site of the UvrA Δ118–419 structure is vacant, whereas the distal site is occupied by ADP (**Fig. 6a,b**). This is in contrast to the open tray structure, in which ADP is found in both nucleotide binding sites[13] (**Supplementary Table 2**). Biochemical analysis confirms that the unique asymmetric nucleotide state observed in the UvrA Δ118–419 structure is also present in full-length UvrA in solution (**Supplementary Fig. 4b**), suggesting that the crystal has captured an authentic intermediate. Second, in the UvrA Δ118–419 structure, the signature domain II has undergone a rigid body rotation of ~16° away from the associated ATP binding domain I in comparison to its position in the open tray structure (**Fig. 6** and **Supplementary Fig. 5**; see also **Supplementary Discussion** and **Supplementary Movie 3**). The nature and coordinated occurrence of these two differences suggest that ATP hydrolysis and release of nucleotide at the proximal site of UvrA mediate a conformational change in signature domain II, analogous to effects seen in other ABC proteins (**Supplementary Figure 8**).

Rotation of the signature domain II as observed in this new structure is predicted to disrupt the nexus of contacts between UvrA and both UvrB and DNA that is described above (**Figs. 3** and **5**). Superposition of the UvrA Δ118–419 structure onto the AB structure predicts a severe clash between the position of UvrB and the signature domain II in the rotated configuration (**Fig. 6f**). Superposition of the UvrA Δ118–419 structure onto the related open tray conformation of UvrA reveals that the position of residues that are implicated in binding to DNA are repositioned in such a way that the new conformation is not likely to be competent to bind lesion DNA. For example, the distance between Arg708 (identified above as a critical contact to DNA, **Fig. 3a**) and the phosphate backbone of lesion-containing DNA taken from the *Thermotoga maritima* UvrA–DNA complex[7] increases by 50% from 8.5 Å to 12.6 Å (additional details in **Supplementary Table 3**). Notably, the orientation of the signature domain II in the UvrA-damaged DNA complex shows a conformation that differs from the conformation in the DNA-free open tray UvrA structure and from our new UvrA Δ118–419 structure. This result lends further support to the idea that the signature domain II undergoes conformational switching during NER.

If the rotation of signature domain II is a consequence of nucleotide hydrolysis and release, mutations that abolish nucleotide binding at the relevant site should phenocopy the nucleotide-deficient state captured by the UvrA Δ118–419 structure. We therefore analyzed the K37A UvrA mutant, in which binding of nucleotide in the proximal site, adjacent to signature domain II, was specifically eliminated. UvrA K37A is indeed defective in its association with UvrB, as indicated by anomalous migration of the AB complex in a size-exclusion column in comparison to wild type (**Fig. 6d**). The affinity of UvrA K37A for lesion-containing DNA is not substantially perturbed (data not shown), probably because the extensive interface between UvrA and DNA is still intact (**Fig. 3** and ref. 7). Thus, dissociation of UvrA from the DNA might require additional structural changes (for example, complete dissociation of the UvrA dimer[21,32]).

Taken together, the predicted disruptions induced by rotation of the signature domain II could result in eviction of UvrA from the UvrA–UvrB–lesion DNA complex, as is required for transition to the UvrB–lesion DNA pre-incision complex (stage 2 to stage 3, **Fig. 1b** and Discussion).

DISCUSSION

Interconversion of two dimers of UvrA during genome scanning

The precise mechanism used by the NER pathway to discriminate native from damaged DNA during scanning of the genome for lesions (**Fig. 1b**, stage 1) is not known. Comparisons of the affinity of native DNA to UvrA with those of a variety of lesion-containing DNAs reveals a relatively small (approximately two- to five-fold) difference (refs. 12,33 and unpublished data). Such a difference is probably not large enough to explain the discrimination of lesion-containing DNA from the vast excess of native DNA. To better explain the discrimination, some have proposed the involvement of kinetic proofreading, whereby productive and nonproductive binding events are distinguished by coupling to appropriate conformational changes and/or nucleotide hydrolysis[2,34,35]. Our findings support such a possibility, and they define the possible conformational changes for the first time. We show that UvrA can adopt two different conformations with substantially different DNA binding surfaces that either permit or preclude binding of lesion DNA. Interconversion between these two states could be an important feature of the mechanism for discriminating damage from native DNA. Specifically, rapid genome scanning would be attributable to cycles of narrowing and widening of the UvrA DNA binding surface (**Fig. 7a** and **Supplementary Fig. 6**). Because genome scanning is known to require ATP binding and hydrolysis, and because our data argue for
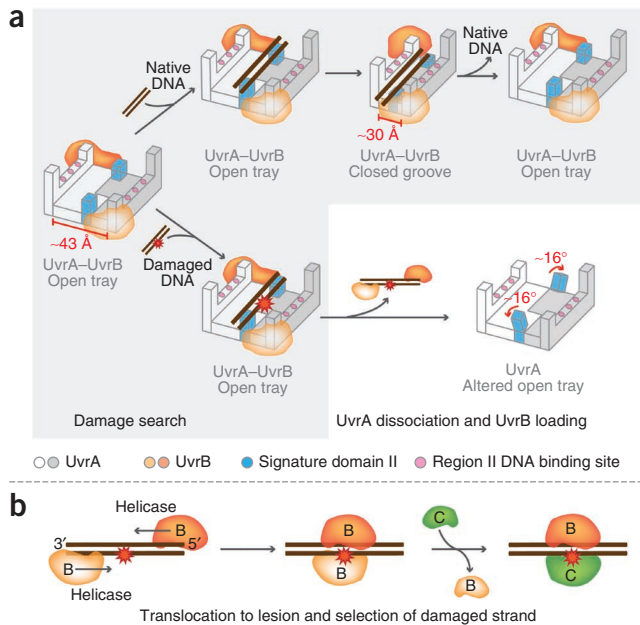
Figure 7 Three distinct conformations of UvrA imply a detailed model for the early events of NER. (**a**) Model of damage search and recognition. (**b**) A model for UvrB loading (see also **Supplementary Figure 9**).

a primary role for the proximal site in regulating interactions among UvrA, UvrB and DNA, we speculate that interconversion between states is associated with nucleotide dynamics at the distal site. We suggest that the initial contact with genomic DNA is made by the open tray form of the AB complex, whose binding surface can accommodate native DNA as well as a wide variety of damaged DNA (**Fig. 4** and ref. 7). These encounters trigger conversion to the closed groove state. In the presence of native DNA, the binding surface would complete this conversion, thus signaling that the just-sampled DNA is native and triggering its release. Concomitantly, UvrA would revert to the open tray conformation in preparation for the next encounter with DNA. Such nonproductive complexes would be predicted to be short-lived and unstable, properties that are exactly like those seen in solution measurements[32,36]. An important consequence of our work is that it shows that UvrA not only selects damaged DNA for further processing but also rejects native DNA (by virtue of its shape) from inappropriate repair.

Encounters with damaged DNA, however, would result in a completely different set of events. Because closure of the DNA binding surface would be blocked by the deformed duplex, UvrA would become trapped in the open tray conformation, resulting in more stable protein–DNA complexes, which have also been observed[32]. The resulting productive complex would then be committed to progressing down the damage-repair pathway (**Fig. 7a** and **Supplementary Fig. 6**).

Eviction of UvrA from the sensor complex

As NER proceeds beyond the initial damage-recognition step, two important events occur concomitantly: dissociation of UvrA from the complex and translocation of UvrB to replace UvrA at the lesion (**Fig. 7a** and **Supplementary Fig. 6**). Insight into the first of these events is provided by analysis of the highly conserved signature domain II of UvrA. The architecture of the interface between UvrA and UvrB in the AB complex, in combination with our analysis of the DNA binding surface of UvrA, reveal that this domain mediates a critical nexus of contacts to UvrB and to DNA and is located adjacent to the proximal ATP binding site (**Figs. 3** and **5**). Our new structure of UvrA shows an altered signature domain II

conformation and a vacant proximal nucleotide binding site (**Fig. 6a,b**). The nature of these features suggests that the altered conformation of the signature domain II would render UvrA unable to bind either UvrB or DNA. Biochemical studies imply that UvrA exits the AB complex after lesion recognition[6]. In this context, our findings suggest that this step of NER is driven by an ATP hydrolysis–dependent conformational change in the signature domain II of UvrA, a change from that seen in the AB structure to that seen in our new UvrA Δ118–419 structure. UvrA eviction would convert an AB complex bound to damaged DNA to an entity containing only UvrB and damaged DNA, setting the stage for transit of UvrB to the lesion, as discussed below.

UvrB in the AB complex is located ~80 Å away from the lesion

The current findings also have implications for the second aspect of the post-lesion-binding transition: replacement of UvrA by UvrB at the lesion position. Until now, there has been no information regarding the spatial disposition of UvrBs relative to the central UvrA dimer. It is notable that within the AB structure, UvrB is located ~80 Å from the expected position of the UvrA-bound lesion (**Fig. 3b**). It was previously envisioned that UvrB and the lesion site would be intimately associated, with replacement of UvrA by UvrB at the appropriate time achieved by remodeling the ensemble[37]. Our results instead imply that UvrB is initially positioned far from the lesion, and thus, in transiting to that site, it must undergo long-range movement. The alternative scenario, in which long-distance movement is achieved by a global conformational change, seems considerably more complicated and therefore unlikely (**Supplementary Fig. 7**). We propose that UvrB moves from its initial peripheral location to the site of damage through its 5′→3′ helicase and single-strand DNA translocase activity[38]. This hypothesis is supported by the existence of intermediate protein–DNA complexes that precede the damage-specific UvrB–DNA complex[12,39]. Moreover, a mutation in UvrB that abolishes helicase and translocase activity shows specific defects in the later steps of NER[16,40], which is consistent with the role proposed here.

The current results also raise two additional issues not previously suspected. First, although two UvrB molecules occupy symmetric positions within the AB complex, the complex in stage 3 of the NER pathway contains a single copy of UvrB, and it is necessarily asymmetric. It is also well established that a single copy of UvrB bound tightly to the lesion and to the UvrC nuclease[20] specifies the geometry of the dual incisions on the lesion-containing strand[37]. First, how is a two-fold symmetric arrangement in the damage-bound A_2B_2 complex (stage 2) transformed into an asymmetric complex in which a single molecule of UvrB is bound specifically around the lesion site (stage 3)? Second, the number and disposition of UvrB in the AB complex imply that the two molecules will bind to opposite strands distant from, and on either side of, the lesion. How then is the lesion-containing strand identified for repair? We propose an economical explanation that addresses these issues (**Fig. 7b** and **Supplementary Fig. 6**). The two-fold symmetry match between the A_2B_2 complex and the duplex DNA implies that the two UvrB molecules could both be loaded onto DNA in opposite orientations on opposite strands of the duplex. Eviction of UvrA would leave these two molecules distant from the lesion. Because each UvrB translocates along one strand of DNA[38,41], the two molecules could then both track along DNA, on their respective strands, toward the lesion and toward each other. Convergence of the two UvrB molecules around the lesion site could be facilitated by the known property of UvrB to dimerize on its C-terminal domain[42]. The intrinsic asymmetry of damaged DNA, in which the lesion is located on one strand of the duplex (**Fig. 1**), could direct the final asymmetric configuration of the UvrB dimer on DNA. This asymmetric dimer would then direct loading of UvrC onto the correct strand, with concomitant loss of one of the two UvrB molecules[20] (**Fig. 7b** and **Supplementary Fig. 6**).

METHODS

Methods and any associated references are available in the online version of the paper at http://www.nature.com/nsmb/.

Note: Supplementary information is available on the Nature Structural & Molecular Biology website.

AUTHOR CONTRIBUTIONS

D.P. purified, crystallized and determined the structure of the AB complex, measured the SAXS data, and carried out DNA binding and UvrA-UvrB interaction studies. M.A.S. solved the structure of UvrA Δ118–419 and did filter binding assays. K.S. prepared UvrB mutants and analyzed their interaction with UvrA. J.H. assisted in protein purification. D.P. and D.J. analyzed the data and wrote the manuscript.

COMPETING FINANCIAL INTERESTS

The authors declare no competing financial interests.

1. Jemal, A., Siegel, R., Xu, J. & Ward, E. Cancer statistics, 2010. *CA Cancer J. Clin.* **60**, 277–300 (2010).
2. Sancar, A. & Reardon, J.T. Nucleotide excision repair in *E. coli* and man. *Adv. Protein Chem.* **69**, 43–71 (2004).
3. Gillet, L.C. & Schärer, O.D. Molecular mechanisms of mammalian global genome nucleotide excision repair. *Chem. Rev.* **106**, 253–276 (2006).
4. Schärer, O.D. Hot topics in DNA repair: the molecular basis for different disease states caused by mutations in TFIIH and XPG. *DNA Repair (Amst.)* **7**, 339–344 (2008).
5. Truglio, J.J., Croteau, D.L., Van Houten, B. & Kisker, C. Prokaryotic nucleotide excision repair: the UvrABC system. *Chem. Rev.* **106**, 233–252 (2006).
6. Orren, D.K. & Sancar, A. The (A)BC excinuclease of *Escherichia coli* has only the UvrB and UvrC subunits in the incision complex. *Proc. Natl. Acad. Sci. USA* **86**, 5237–5241 (1989).
7. Jaciuk, M., Nowak, E., Skowronek, K., Tanska, A. & Nowotny, M. Structure of UvrA nucleotide excision repair protein in complex with modified DNA. *Nat. Struct. Mol. Biol.* **18**, 191–197 (2011).
8. Truglio, J.J. *et al.* Structural basis for DNA recognition and processing by UvrB. *Nat. Struct. Mol. Biol.* **13**, 360–364 (2006).
9. Eryilmaz, J. *et al.* Structural insights into the cryptic DNA-dependent ATPase activity of UvrB. *J. Mol. Biol.* **357**, 62–72 (2006).
10. Waters, T.R., Eryilmaz, J., Geddes, S. & Barrett, T.E. Damage detection by the UvrABC pathway: crystal structure of UvrB bound to fluorescein-adducted DNA. *FEBS Lett.* **580**, 6423–6427 (2006).
11. Oh, E.Y., Claassen, L., Thiagalingam, S., Mazur, S. & Grossman, L. ATPase activity of the UvrA and UvrAB protein complexes of the *Escherichia coli* UvrABC endonuclease. *Nucleic Acids Res.* **17**, 4145–4159 (1989).
12. Bertrand-Burggraf, E., Selby, C.P., Hearst, J.E. & Sancar, A. Identification of the different intermediates in the interaction of (A)BC excinuclease with its substrates by DNase I footprinting on two uniquely modified oligonucleotides. *J. Mol. Biol.* **219**, 27–36 (1991).
13. Pakotiprapha, D. *et al.* Crystal structure of *Bacillus stearothermophilus* UvrA provides insight into ATP-modulated dimerization, UvrB interaction, and DNA binding. *Mol. Cell* **29**, 122–133 (2008).
14. Timmins, J. *et al.* Structural and mutational analyses of *Deinococcus radiodurans* UvrA2 provide insight into DNA binding and damage recognition by UvrAs. *Structure* **17**, 547–558 (2009).
15. Rossi, F. *et al.* The biological and structural characterization of *Mycobacterium tuberculosis* UvrA provides novel insights into its mechanism of action. *Nucleic Acids Res.* **39**, 7316–7328 (2011).
16. Seeley, T.W. & Grossman, L. The role of *Escherichia coli* UvrB in nucleotide excision repair. *J. Biol. Chem.* **265**, 7158–7165 (1990).
17. Wagner, K., Moolenaar, G.F. & Goosen, N. Role of the insertion domain and the zinc-finger motif of *Escherichia coli* UvrA in damage recognition and ATP hydrolysis. *DNA Repair (Amst.)* **10**, 483–496 (2011).
18. Doolittle, R.F. *et al.* Domainal evolution of a prokaryotic DNA repair protein and its relationship to active-transport proteins. *Nature* **323**, 451–453 (1986).
19. Pakotiprapha, D., Liu, Y., Verdine, G.L. & Jeruzalmi, D. A structural model for the damage-sensing complex in bacterial nucleotide excision repair. *J. Biol. Chem.* **284**, 12837–12844 (2009).
20. Verhoeven, E.E., Wyman, C., Moolenaar, G.F. & Goosen, N. The presence of two UvrB subunits in the UvrAB complex ensures damage detection in both DNA strands. *EMBO J.* **21**, 4196–4205 (2002).
21. Malta, E., Moolenaar, G.F. & Goosen, N. Dynamics of the UvrABC nucleotide excision repair proteins analyzed by fluorescence resonance energy transfer. *Biochemistry* **46**, 9080–9088 (2007).
22. Moolenaar, G.F., Schut, M. & Goosen, N. Binding of the UvrB dimer to non-damaged and damaged DNA: residues Y92 and Y93 influence the stability of both subunits. *DNA Repair (Amst.)* **4**, 699–713 (2005).
23. Guinier, A. & Fournet, G. Xxxxxxx. in *Small-angle scattering of X-rays* (Wiley, New York, 1955).
24. Svergun, D. Determination of the regularization parameter in indirect-transform methods using perceptual criteria. *J. Appl. Crystallogr.* **25**, 495–503 (1992).
25. Wriggers, W. Using Situs for the integration of multi-resolution structures. *Biophys Rev.* **2**, 21–27 (2010).
26. Chen, J., Lu, G., Lin, J., Davidson, A.L. & Quiocho, F.A. A tweezers-like motion of the ATP-binding cassette dimer in an ABC transport cycle. *Mol. Cell* **12**, 651–661 (2003).
27. Davidson, A.L. & Chen, J. ATP-binding cassette transporters in bacteria. *Annu. Rev. Biochem.* **73**, 241–268 (2004).
28. Rees, D.C., Johnson, E. & Lewinson, O. ABC transporters: the power to change. *Nat. Rev. Mol. Cell Biol.* **10**, 218–227 (2009).
29. Lammens, K. *et al.* The Mre11:Rad50 structure shows an ATP-dependent molecular clamp in DNA double-strand break repair. *Cell* **145**, 54–66 (2011).
30. Truglio, J.J. *et al.* Interactions between UvrA and UvrB: the role of UvrB's domain 2 in nucleotide excision repair. *EMBO J.* **23**, 2498–2509 (2004).
31. Hsu, D.S., Kim, S.T., Sun, Q. & Sancar, A. Structure and function of the UvrB protein. *J. Biol. Chem.* **270**, 8319–8327 (1995).
32. Thiagalingam, S. & Grossman, L. The multiple roles for ATP in the *Escherichia coli* UvrABC endonuclease-catalyzed incision reaction. *J. Biol. Chem.* **268**, 18382–18389 (1993).
33. Croteau, D.L. *et al.* The C-terminal zinc finger of UvrA does not bind DNA directly but regulates damage-specific DNA binding. *J. Biol. Chem.* **281**, 26370–26381 (2006).
34. Ninio, J. Kinetic amplification of enzyme discrimination. *Biochimie* **57**, 587–595 (1975).
35. Hopfield, J.J. Kinetic proofreading: a new mechanism for reducing errors in biosynthetic processes requiring high specificity. *Proc. Natl. Acad. Sci. USA* **71**, 4135–4139 (1974).
36. Kad, N.M., Wang, H., Kennedy, G.G., Warshaw, D.M. & Van Houten, B. Collaborative dynamic DNA scanning by nucleotide excision repair proteins investigated by single-molecule imaging of quantum-dot-labeled proteins. *Mol. Cell* **37**, 702–713 (2010).
37. Van Houten, B. Nucleotide excision repair in *Escherichia coli. Microbiol. Rev.* **54**, 18–51 (1990).
38. Oh, E.Y. & Grossman, L. Characterization of the helicase activity of the *Escherichia coli* UvrAB protein complex. *J. Biol. Chem.* **264**, 1336–1343 (1989).
39. Moolenaar, G.F., Visse, R., Ortiz-Buysse, M., Goosen, N. & van de Putte, P. Helicase motifs V and VI of the *Escherichia coli* UvrB protein of the UvrABC endonuclease are essential for the formation of the preincision complex. *J. Mol. Biol.* **240**, 294–307 (1994).
40. Orren, D.K. & Sancar, A. Formation and enzymatic properties of the UvrB.DNA complex. *J. Biol. Chem.* **265**, 15796–15803 (1990).
41. Oh, E.Y. & Grossman, L. Helicase properties of the *Escherichia coli* UvrAB protein complex. *Proc. Natl. Acad. Sci. USA* **84**, 3638–3642 (1987).
42. Hildebrand, E.L. & Grossman, L. Oligomerization of the UvrB nucleotide excision repair protein of *Escherichia coli. J. Biol. Chem.* **274**, 27885–27890 (1999).
43. Park, H. *et al.* Crystal structure of a DNA decamer containing a *cis*-syn thymine dimer. *Proc. Natl. Acad. Sci. USA* **99**, 15965–15970 (2002).
44. Yeh, H.J. *et al.* NMR solution structure of a nonanucleotide duplex with a dG mismatch opposite a 10S adduct derived from *trans* addition of a deoxyadenosine N6-amino group to (+)-(7R,8S,9S,10R)-7,8-dihydroxy-9,10-epoxy-7,8,9,10- tetra-hydrobenzo[a]pyrene: an unusual syn glycosidic torsion angle at the modified dA. *Biochemistry* **34**, 13570–13581 (1995).
45. Zaliznyak, T., Bonala, R., Johnson, F. & de Los Santos, C. Structure and stability of duplex DNA containing the 3-(deoxyguanosin-N2-yl)-2-acetylaminofluorene (dG(N2)-AAF) lesion: a bulky adduct that persists in cellular DNA. *Chem. Res. Toxicol.* **19**, 745–752 (2006).
46. McAteer, K., Jing, Y., Kao, J., Taylor, J.S. & Kennedy, M.A. Solution-state structure of a DNA dodecamer duplex containing a *cis*-syn thymine cyclobutane dimer, the major UV photoproduct of DNA. *J. Mol. Biol.* **282**, 1013–1032 (1998).

ONLINE METHODS

Protein biochemistry and crystallization. *Geobacillus stearothermophilus* UvrA and UvrB were purified as described[13] (**Supplementary Methods**). The AB complex was formed by mixing UvrA with a two-fold molar excess of UvrB at 10–20 µM UvrA concentration in 20 mM Tris-HCl, pH 7.5, 150 mM NaCl, 5% (v/v) glycerol, 5 mM β-ME. The mixture was concentrated to approximately 50 µM, at which point 5 mM $MgCl_2$ and 2 mM ATPγS were added. The complex was purified by size-exclusion chromatography (Superdex 200; GE Healthcare; 20 mM Tris-HCl, pH 7.5, 150 mM NaCl, 5% (v/v) glycerol, 5 mM β-ME, 5 mM $MgCl_2$ and 2 mM ATP).

Crystals of the AB complex were grown using the sitting drop vapor diffusion method at 22 °C. The crystallization drop consisted of a 1:1 mixture of protein (24 mg ml^{-1}) and reservoir solution (90 mM sodium-potassium phosphate, pH 6.5, 180 mM NaCl, 22.5% (w/v) PEG 1000, 5% (w/v) trehalose dihydrate). For the cryogenic X-ray diffraction, the crystals were serially transferred to a 10-µl drop of crystallization buffer containing 10%, 15% and 19% (w/v) trehalose dihydrate and flash frozen in liquid nitrogen.

UvrA Δ118–419 was crystallized using the hanging-drop vapor diffusion method at 4 °C. The crystallization drop consisted of a 1:1 mixture of protein (6–12 mg ml^{-1}) and reservoir solution (100 mM BICINE, pH 9.0, 5% (v/v) 1,4-dioxane, 3% (w/v) PEG 20,000) in the presence of 5 mM AMP-PCP and 10 mM $MgCl_2$. Prior to X-ray diffraction, the crystals were soaked in 15 mM AMP-PCP, 15 mM ADP, 60 mM $MgCl_2$ and 20% (v/v) glycerol for 3 h and flash frozen in liquid nitrogen.

Structure determination. X-ray diffraction data were collected at the NE-CAT beamlines 24ID-C and 24ID-E (λ = 0.97919 Å) and processed using HKL2000 (ref. 47).

The AB complex crystallized in space group $P4_22_12$ with cell parameters $a = b = 216.8$ Å, $c = 116.8$ Å, $\alpha = \beta = \gamma = 90.0°$, and contained one molecule each of UvrA and UvrB in the asymmetric unit. The structure was solved at 4.4 Å by molecular replacement (PHASER)[48], using the structures of the isolated components as search models (chain A of PDB 2R6F[13] for UvrA and PDB 1T5L[30] for UvrB). Crystallographic refinement was carried in CNS[49,50] and Phenix[51]. The final model consists of residues 1–309 and 314–949 of UvrA and residues 1–595 of UvrB with a crystallographic R factor of 28.76% and R_{free} of 34.86%. The accuracy of the AB structure was confirmed by a Fourier analysis in which the crystallographic phases from the refined model were applied to anomalous diffraction data collected from the AB complex in which UvrA alone had been substituted with selenomethionine. Data collection and refinement statistics can be found in **Table 1**. Details of the crystallographic refinement and model validation can be found in **Supplementary Methods**.

UvrA Δ118–419 crystallized in the monoclinic space group $C2$ with unit cell dimensions $a = 128.7$ Å, $b = 51.3$ Å, $c = 112.4$ Å, $\alpha = \gamma = 90°$, $\beta = 97.3°$, and one UvrA molecule in the asymmetric unit. The structure was solved at 2.1-Å resolution by molecular replacement using PHASER[48] and a search model that included the four relevant domains from the full-length UvrA structure (PDB 2R6F): ATP binding domain I, ATP binding domain II, signature domain I and signature domain II. The model was refined using CNS[50] and REFMAC[52]. The refinement converged on a crystallographic R factor of 21.05% and an R_{free} of 24.53%. The final model contains residues 2–56, 72–90, 95–105, 433–434, 461–744 and 757–949, with one ADP molecule bound to the distal nucleotide binding site. Data collection and refinement statistics can be found in **Table 1**.

Structural analysis. Structural analysis and visualization were carried out using the CCP4 software package[53] and PyMOL (Delano Scientific). Motion analysis of the signature domain II of UvrA and of the conformational changes in ABC proteins in different nucleotide states was done using DynDom[54,55]. Determination of the helical rotation describing the conformational changes of UvrA protomers upon rearrangement from the open tray state (PDB 2R6F) to the closed groove state (UvrA within the AB complex) was carried out using LSQMAN[56]. A detailed description of the UvrA structures included in the analysis can be found in **Supplementary Methods**.

Small-angle X-ray scattering. SAXS data were measured at three different concentrations of the UvrA–UvrB complex (1, 2 and 4 mg ml^{-1}) at the Bio-CAT beamline 18ID-D. Data were processed in IGOR Pro (WaveMetrics) using scripts developed by the Bio-CAT staff and the ATSAS software package[57]. The pair distribution function was calculated using GNOM[24]. The *ab initio* envelope reconstructions were carried out in DAMMIN and DAMAVER[58,59]. The theoretical R_g of the crystal structure was calculated in CRYSOL[60]. The crystal structure of the A_2B_2 heterotetramer was docked into the SAXS-derived molecular envelope using SITUS 2.5 (ref. 25).

Filter binding assay. The binding reactions contained 0.2–5.0 µM of wild-type or mutant UvrA proteins and [α-^{32}P]ATP in the context of 1 µM unlabeled ATP. The reaction buffer consisted of 20 mM K-HEPES, pH 7.5, 100 mM KCl, 15 mM $MgCl_2$, 2 mM DTT, 5% (v/v) glycerol and 50 µg ml^{-1} bovine serum albumin. The reactions were incubated for 30 min at 55 °C. After incubation, the reactions were placed on ice and then applied to a nitrocellulose membrane, which was subsequently exposed to a phosphorscreen and quantified using ImageQuant TL (GE Healthcare).

Isothermal titration calorimetry. ITC was carried out using an ITC200 (Microcal). UvrA and UvrB were buffer exchanged into 10 mM Na-HEPES, pH 7.5, 100 mM NaCl, 5 mM $MgCl_2$, 1 mM ATP, using a PD-10 desalting column (GE Healthcare). Titration was done by injecting 25 consecutive aliquots of UvrB (91.8 µM) into the ITC cell containing UvrA (5.16 µM) at 30 °C. The volume of each injection was 0.5 µl for the first two injections and 1.5 µl for the following 23 injections. Binding stoichiometry, enthalpy and equilibrium dissociation constants were determined by fitting the data to a single set of identical sites model using Origin 7 (Microcal).

Analysis of UvrA-UvrB interaction, electrophoretic mobility shift assay and ATPase assay. Interaction between UvrA and UvrB was analyzed by size-exclusion chromatography, and DNA binding by UvrA mutants was analyzed by electrophoretic mobility shift assay, as described[13,19]. The rate of ATP hydrolysis was measured using a coupled enzyme assay system consisting of pyruvate kinase and lactate dehydrogenase[61]. Detailed experimental procedures are described in **Supplementary Methods**.

47. Otwinowski, Z. & Minor, W. Processing of X-ray diffraction data collected in oscillation mode. *Methods Enzymol.* **276**, 307–326 (1997).
48. McCoy, A.J. *et al.* Phaser crystallographic software. *J. Appl. Crystallogr.* **40**, 658–674 (2007).
49. Schröder, G.F., Levitt, M. & Brunger, A.T. Super-resolution biomolecular crystallography with low-resolution data. *Nature* **464**, 1218–1222 (2010).
50. Brünger, A.T. *et al.* Crystallography & NMR system: a new software suite for macromolecular structure determination. *Acta Crystallogr. D Biol. Crystallogr.* **54**, 905–921 (1998).
51. Adams, P.D. *et al.* PHENIX: a comprehensive Python-based system for macromolecular structure solution. *Acta Crystallogr. D Biol. Crystallogr.* **66**, 213–221 (2010).
52. Winn, M.D., Murshudov, G.N. & Papiz, M.Z. Macromolecular TLS refinement in REFMAC at moderate resolutions. *Methods Enzymol.* **374**, 300–321 (2003).
53. Winn, M.D. *et al.* Overview of the CCP4 suite and current developments. *Acta. Crystallogr. D. Biol. Crystallogr.* **67**, 235–242 (2011).
54. Hayward, S. & Berendsen, H.J. Systematic analysis of domain motions in proteins from conformational change: new results on citrate synthase and T4 lysozyme. *Proteins* **30**, 144–154 (1998).
55. Hayward, S. & Lee, R.A. Improvements in the analysis of domain motions in proteins from conformational change: DynDom version 1.50. *J. Mol. Graph. Model.* **21**, 181–183 (2002).
56. Kleywegt, G.J. Use of non-crystallographic symmetry in protein structure refinement. *Acta. Crystallogr. D. Biol. Crystallogr.* **52**, 842–857 (1996).
57. Konarev, P., Petoukhov, M.V., Volkov, V. & Svergun, D.I. ATSAS 2.1, a program package for small-angle scattering data analysis. *J. Appl. Crystallogr.* **39**, 277–286 (2006).
58. Svergun, D.I. Restoring low resolution structure of biological macromolecules from solution scattering using simulated annealing. *Biophys. J.* **76**, 2879–2886 (1999).
59. Volkov, V.V. & Svergun, D.I. Uniqueness of *ab initio* shape determination in small-angle scattering. *J. Appl. Crystallogr.* **36**, 860–864 (2003).
60. Svergun, D., Barberato, C. & Koch, M.H.J. CRYSOL-a program to evaluate X-ray solution scattering of biological macromolecules from atomic coordinates. *J. Appl. Crystallogr.* **28**, 768–773 (1995).
61. Kiianitsa, K., Solinger, J.A. & Heyer, W.D. NADH-coupled microplate photometric assay for kinetic studies of ATP-hydrolyzing enzymes with low and high specific activities. *Anal. Biochem.* **321**, 266–271 (2003).